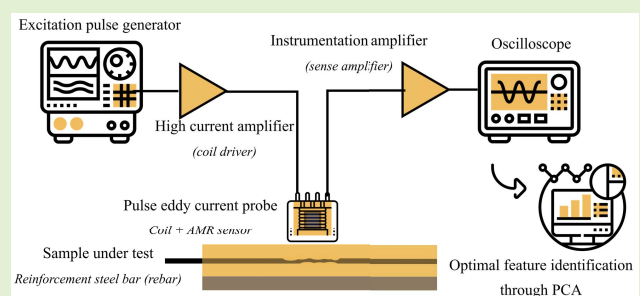


Feature Engineering of Time-Domain Signals Based on Principal Component Analysis for Rebar Corrosion Assessment Using Pulse Eddy Current

Durgesh Tamhane^{ID}, Jinit Patil, Sauvik Banerjee, and Siddharth Tallur^{ID}

Abstract—Corrosion of steel rebars in reinforced concrete impacts structural integrity of the infrastructure. While several Non-Destructive Testing and Evaluation (NDT&E) techniques exist for corrosion monitoring in structures, there is a need for cost-effective solution for early detection of sub-surface corrosion of rebars in civil infrastructure. Here we present a low-cost corrosion sensing system based on pulsed eddy current detection using anisotropic magnetoresistive (AMR) sensor to detect the corrosion in steel reinforcing bars. A novel probe with large figure of merit ($21.62 \times 6 \text{ m T}^{-1}$) is presented, that can detect corrosion in 20 mm diameter rebars at lift-off distances as high as 55 mm with low excitation current of 0.2 A. The sensitivity is enhanced by using area under the curve of various segments of the time-domain sensor output as features. Optimal feature selection and dimensionality reduction, as well as quantitative estimation of extent of corrosion are demonstrated using principal component analysis.



Index Terms—Pulsed eddy current, AMR sensor, rebar corrosion, feature extraction, principal component analysis.

I. INTRODUCTION

RINFORCEMENT steel bars (rebars) added in concrete structures to increase their tensile strength are susceptible to corrosion [1], [2]. As the rebars corrode, the service life of the reinforced concrete (RC) structures reduces significantly leading to premature failure. The global cost of maintenance and repairs of corroded structures is estimated to be upwards of USD\$2.5 trillion worldwide [3]. The conventional standard test method for corrosion potentials of uncoated reinforcing

steel in concrete (ASTM C876-15) [4] leverages half-cell potential measurement. However, this technique provides only a probabilistic estimate of occurrence of corrosion over an area at the time of measurement [5], and is not amenable to quantitative assessment. With global warming, limited access to appropriate resources for construction of new infrastructure and increase in corrosive environments will lead to accelerated deterioration of concrete infrastructure affecting their durability and serviceability [6], [7]. A number of non-destructive evaluation (NDE) techniques have been investigated to evaluate concrete integrity [8].

Electromagnetic techniques such as connectionless electrical pulse response analysis (CEPRA) and pulsed eddy current (PEC) are promising non-invasive test methods that offer high sensitivity [9]. PEC has been extensively used for detection of corrosion in oil & gas and water pipelines [10]–[13]. The capability of PEC technique to detect defects deep inside the test material due to the broad frequency spectrum of the excitation signal makes it the most versatile and popular NDE technique for inspection of ferromagnetic materials, such as steel pipelines [14]. The PEC method utilizes time-varying magnetic field produced by an electromagnetic excitation coil to generate eddy currents in an electrically conducting sample.

Manuscript received July 9, 2021; revised August 4, 2021; accepted August 5, 2021. Date of publication August 9, 2021; date of current version October 1, 2021. This work was supported in part by the Department of Science & Technology, Government of India, through IMPRINT-2A under Grant IMP/2018/001442 and in part by the Sanrachana Structural Strengthening Pvt., Ltd., under Grant RD/0119-SSIMPQ2-001. The associate editor coordinating the review of this article and approving it for publication was Prof. Guiyun Tian. (Corresponding author: Siddharth Tallur.)

Durgesh Tamhane, Jinit Patil, and Siddharth Tallur are with the Department of Electrical Engineering, Indian Institute of Technology (IIT) Bombay, Mumbai, Maharashtra 400076, India (e-mail: stallur@ee.iitb.ac.in).

Sauvik Banerjee is with the Department of Civil Engineering, Indian Institute of Technology (IIT) Bombay, Mumbai, Maharashtra 400076, India (e-mail: sauvik@civil.iitb.ac.in).

Digital Object Identifier 10.1109/JSEN.2021.3103545

The eddy currents produced in the sample generate their own secondary magnetic field, that opposes the primary field generated by the excitation coil. In response to a pulse excitation field, the secondary field exhibits a decaying exponential signature, with time-constant proportional to the conductivity of the sample [15]. The decaying exponential profile is affected by the thickness, conductivity and permeability of the sample and the distance of the sample from the sensing element (lift-off), and can therefore be utilized to estimate the extent of corrosion in the sample. Traditional signal processing methods employed on PEC sensor output used to estimate corrosion use signal features such as peak value [16], peak arrival time [17], [18], rise time [19], time to peak [20] and zero crossing time [21]. In recent years, newer signal features have been reported, including slope of a piece-wise-linear representation of the falling edge of the PEC sensor output [22], [23] to realize sample detection at large lift-off. Time slice integrals (TSIs) of the PEC sensor output computed in individual time windows have also been reported as features sensitive to corrosion in casing-pipe monitoring [24]. Given various uncorrelated features, it is possible to combine several features and leverage principal component analysis (PCA) [25], [26] to determine suitable features for detecting corrosion. Commercially available PEC testing systems e.g. Eddyfi [27], Maxwell NDT [28] and Applus+ RTD INCOTEST™ [29] typically utilize features such as log-linear slope (decay rate) and characteristic time (decay time) of the decaying portion of the sensor output time-series to detect and assess corrosion.

Employing PEC sensing for corrosion detection in steel rebars embedded in concrete presents additional challenges as compared to the use-case of pipeline monitoring. The steel surface of the pipelines to be inspected is often exposed or has minimal insulation. Rebars are however buried at large depths, 40 mm or higher, inside concrete, in case of reinforced cement concrete (RCC) structures. Additionally, the surface area of the ferromagnetic material probed with the PEC sensor is much larger in steel pipelines than rebars, that typically have diameters of few centimetres. Nevertheless, some attempts have been made to use PEC testing for inspection of rebars in concrete. Ulapane *et al.* [30] reported a coil-based PEC sensor for rebar localization within a concrete structure and determination of thickness of the concrete cover by analyzing the time varying voltage output of the sensor. With this technique the authors could detect the reinforcement rods at a maximum depth of 50 mm. However, no attempt was made to investigate the effect of corrosion of the rebars on the PEC signal. Eddy *et al.* [15] have employed a commercially available PEC instrument to differentiate rebars of various diameters with lift-off (separation of rebar from PEC probe) upto 100 mm by analyzing the intercepts of best-fit lines on the time-domain response signal of the PEC detection coil [15], [23]. The authors have not investigated the feasibility of applying this technique for early identification of corrosion in rebars embedded in concrete. Structural health monitoring of mechanical and aerospace structures is mostly similar worldwide, but monitoring of civil infrastructure varies due to socio-economic, cultural, geographical, and governmental reasons across countries, and

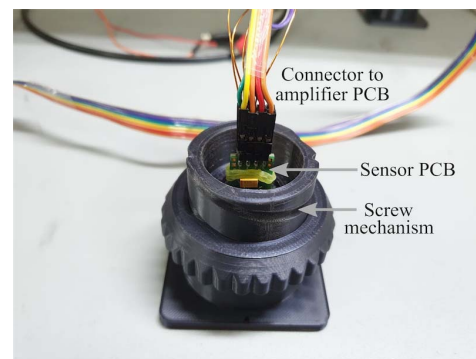


Fig. 1. Photograph of the PEC probe. The screw mechanism is used to introduce lift-off for characterization of sensor performance.

even across states within the same country [31]. Development of low-cost monitoring solutions for early detection of rebar corrosion will greatly improve the efficiency of infrastructure construction and repairs, especially in populous developing countries. While numerous reports of low-cost PEC probe designs are available in literature [16], [22], [26], [32]–[40], the maximum reported lift-off distances are not adequate for detecting RCC rebar corrosion.

In this work, we report a novel probe construction that enables detection of corroded rebars at large lift-off (up to 55 mm) with low current (0.2 A). This sensitivity is achieved using (i) coaxial probe design comprising of an excitation coil and a high resolution anisotropic magneto-resistive (AMR) sensor used as a detector, and (ii) utilizing PCA to determine the appropriate time-slices to compute integrated time domain response of the sensor (i.e. area under the curve (AUC) of the time domain signal), that are used as features to distinguish corroded portions of a rebar from non-corroded portions. The AUC captures the effect of formation of corrosion byproducts and volume loss due to corrosion by accounting for all the decaying eddy current transients in the sample under the influence of a current pulse in the excitation coil. We employ PCA to determine the segments of the curve that are most sensitive to corrosion of the sample, and enhance the sensitivity of the system by quantifying the state of corrosion through the most significant principal components.

II. METHODS

A. Pulsed Eddy Current (PEC) Probe

The PEC probe is designed to be portable, and in a form suitable for implementing an integrated scanning probe (Figure 1). The 3D printed holder houses the excitation coil and an AMR sensor (Honeywell HMC1001). AMR sensors typically have high sensitivity (order of few mV/V/Gauss used in a Wheatstone bridge configuration) and can be used to detect weak magnetic fields [41]–[43]. A 3D printed cylindrical holder is used as a PEC probe. The probe holder has a screw mechanism to raise the separation between the sample and the AMR sensor, for characterization of sensor performance with lift-off. Note that lift-off as mentioned in the results presented subsequently, refers to the ‘design lift-off’ i.e. separation between the bottom surface of the probe and surface of the rebar closest to the probe. The assembly has a vertical slot that houses the AMR

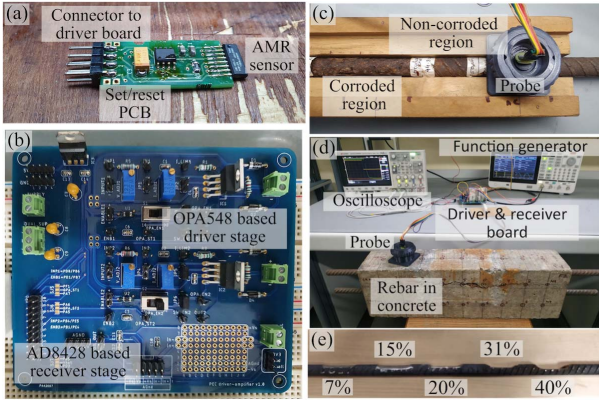


Fig. 2. (a) Photograph of AMR sensor interface PCB. (b) Photograph of driver and receiver interface PCB. The coil driver stage comprises of a Texas Instruments OPA548 amplifier based high current driver stage amplifier, and an Analog Devices AD8428 instrumentation amplifier (receiver) for the AMR sensor signal. (c) PEC probe comprising of excitation coil and AMR sensor interface PCB used to interrogate corroded and non-corroded regions on a bare rebar. (d) Photograph of the complete experimental setup used for characterization of rebars embedded in concrete. (e) Photograph of manually chamfered rebar, showing extent of diameter loss in various sections.

sensor PCB, which also includes a power MOSFET (Vishay IRF540) based datasheet recommended set/reset circuit for the HMC1001 (Figure 2(a)). The set/reset circuit is not required in normal operation, and is only useful if the AMR sensor experiences a strong external magnetic field that can re-magnetize the sensor. Copper wire of diameter 0.5 mm is wound on the cylinder to form the excitation coil (90 turns, 30 mm diameter). The coil and AMR sensor are connected to an external PCB that houses the driver amplifier and AMR sensor interface circuits (Figure 2(b)). A high current operational amplifier (Texas Instruments OPA548) is used in non-inverting amplifier configuration with gain = 2 to drive the excitation coil. The circuit design for the OPA548 stage is based on coil excitation circuit reported by Ulapane *et al.* [22]. In order to limit the current in the coil to avoid over-heating, a 10 Ω/10 W resistor is connected in series with the coil to the output of OPA548. Flyback diodes are used to protect OPA548 from the back electromotive force (back EMF) generated by the coil. The differential output of the HMC1001 is amplified using an ultra-low noise instrumentation amplifier (Analog Devices AD8428) with gain = 2000. The DC component of the AMR sensor output is eliminated using high pass filter with cut-off frequency 1 Hz. The PCB is connected to an arbitrary function generator (Tektronix AFG31052) to generate the pulse for coil excitation, and an oscilloscope (Keysight DSOX2014A) used to record the excitation pulse and sensor output. The setup is used to characterize bare rebars with lift-off introduced by appropriately adjusting the screw mechanism in the probe (Figure 2(c)) as well as rebars embedded in concrete (Figure 2(d)). To study the variation in sensor output with extent of corrosion, the sensor is tested on a steel rebar of 20 mm diameter that is manually chamfered at 5 separate locations along its length with a metal grinder (Figure 2(e)).

The capability of this PEC sensor is measured by defining a figure of merit (FoM) as the performance metric of the

probe. The magnetic field (B_L) generated by a coil is given by $B_L = \frac{\mu_0 \mu_r I N R^2}{2(R^2 + L^2)^{3/2}}$, where μ_0 is the magnetic permeability of vacuum, μ_r is relative permeability of the core (in this case, air) in the coil, I is the current in the coil, R is the radius of the coil, N is the number of turns of the coil and L is the distance away from the coil where the field is measured. It is desirable to have a coil for PEC testing, that can distinguish corroded samples from uncorroded samples at higher lift-off z with minimal field. Therefore, the figure of merit is defined as:

$$FoM = \frac{z}{B_L} = \frac{2z(R^2 + L^2)^{3/2}}{\mu_0 \mu_r I N R^2} \quad (1)$$

Table I shows a comparison of FoM of the probe used in this work compared to other PEC probes reported in literature. For each probe reported in **Table I**, we have evaluated field at distance $L = 1$ m from the coil for uniform comparison.

B. Area Under the Curve as a Feature for Corrosion Assessment

The decay of the transient voltage response in rebars has the general form [30] $V(t) = \sum_{i=1}^{\infty} C_i e^{-\tau_i t}$, where C_i and τ_i are determined by the gain (sensitivity) of the sensor, and electrical and magnetic properties of any surrounding conductive materials, including the sample under test. The characteristic diffusion times τ_i for the exponents are reported to be related to the magnetic permeability (μ_s) and electrical conductivity (σ_s) of the rebar material, and radius of the rebar (r): $\tau_i \propto \mu_s \sigma_s r^2$ [15], [44]. In recent studies [15], [30], the slope of the sensor response in time domain visualized in log-linear scale is used as a feature to analyze the extent of corrosion, since it accounts for σ_s and r of the rebars, and is thus altered due to corrosion. It is to be noted that the linear region of the logarithm of the acquired detector response is used for analysis in the PEC technique. However, the linear region is also affected by coil parameters and therefore it becomes vital to choose a region of interest such that an appropriate linear fit is obtained. This requires additional calibration and post-processing [30]. In this work, we have used AUC for the analysis of the signal feature. This amounts to integrating the sensor response in a time window that captures the voltage decay, and therefore the AUC accounts for the slope of various linear regions that are discussed in other work [15], [30]. The time window for computing the AUC can be appropriately chosen to be limited to smaller sections of the curve in the region of steepest exponential decay. The sum of exponentials nature of the equation above suggests that multiple such areas of different non-overlapping instances in time can be utilized (e.g. Figure 3) for enhancing the sensitivity of the system at higher lift-off using PCA. Note that the initial portion of the sensor output signal is saturated due to the high gain of the AD8428 sense amplifier. However, the trailing portion of the decaying exponential signal is captured with high resolution, and can be utilized for PCA. When working with areas of multiple sections of the curve, PCA also allows for dimensionality reduction i.e. representation of the state of health of the rebar with few principal components instead of a large number of area calculations.

TABLE I

COMPARISON OF FIGURE OF MERIT (FoM) FOR PULSED EDDY CURRENT DETECTION PROBES REPORTED IN LITERATURE.
TMR: TUNNEL MAGNETO-RESISTIVE SENSOR, AMR: ANISOTROPIC MAGNETO-RESISTIVE SENSOR

Reference	Detector	Excitation coil parameters				Maximum lift-off reported [mm]	FoM [$\times 10^6 \text{ m T}^{-1}$]
		Turns	Diameter [mm]	Current [A]	Core		
Li. et al. [16]	TMR	804	25	0.3	Air	0.5	0.02
Ulapane et al [22]	Coil	600	57	0.2	Air	14	0.23
Nafiah et al. [26]	Coil	210	80	2	Air	12	0.02
Xie et al. [32]	Coil	296	10	2	Air	0	<0.01
Piao et al. [33]	Coil	28	14.20	0.28	Air	3	12.08
Abidin et al. [34]	Coil	400	13.9	0.02	Ferrite	3.25	<0.01
Chen et al. [35]	Coil	198	28.4	0.5	Air	5	0.39
Johnston et al. [36]	Coil	127	13.5	0.17	Air	4.4	7.11
Xie et al. [37]	Coil	304	24	0.3	Air	8	0.97
Angani et al. [38]	Hall sensor	120	26	0.5	Ferrite	8	<0.01
Lebrun et al. [39]	Hall sensor	100	26	1.6	Air	15	0.88
Li et al. [40]	Hall sensor	296	12	1	Air	0.5	0.07
Tsukada et al. [41]	AMR	50	26	0.1	Air	6	11.31
This work	AMR	90	30	0.2	Air	55	21.62

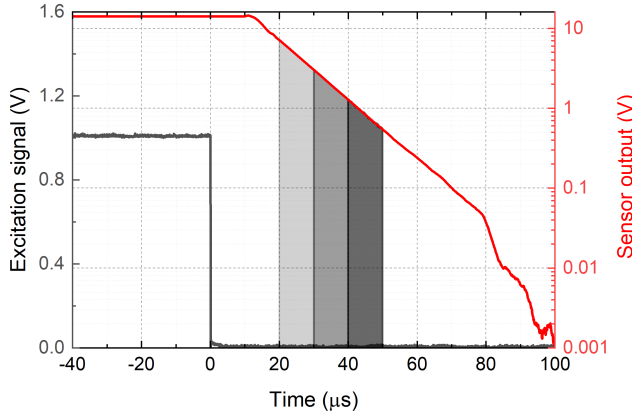


Fig. 3. Area under the curve (of the amplified sensor output signal) is used as a feature to distinguish corroded and non-corroded rebars. Excitation signal and sensor output obtained for corroded rebar with 40 mm lift-off is presented, and area under the curve for segments corresponding to 20-30 μs , 30-40 μs and 40-50 μs are highlighted. The sensor output is displayed in logarithmic scale for easier visualization.

C. Selection of Appropriate Time-Segments for AUC Based on PCA

Consider the AUC for various segments of the time-domain signal, represented as A_j , $j = 1, 2 \dots N$. Here N denotes number of segments under consideration. The principal components obtained through PCA can be represented as $P_i = \sum_{j=1}^N a_{i,j} A_j$, where $a_{i,j}$ denote the factor loadings of the i^{th} principal component and j^{th} feature i.e. AUC segment. The features can be represented by M principal components, subject to the condition $M \leq N$. Therefore this can be represented in matrix form as follows:

$$\begin{pmatrix} P_1 \\ P_2 \\ \vdots \\ P_M \end{pmatrix} = \begin{pmatrix} a_{1,1} & a_{1,2} & \dots & a_{1,N} \\ a_{2,1} & a_{2,2} & \dots & a_{2,N} \\ \vdots & \vdots & \ddots & \vdots \\ a_{M,1} & a_{M,2} & \dots & a_{M,N} \end{pmatrix} \begin{pmatrix} A_1 \\ A_2 \\ \vdots \\ A_N \end{pmatrix} \quad (2)$$

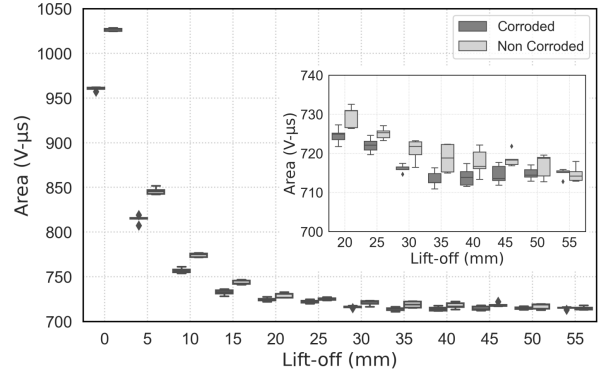


Fig. 4. Variation of area under the curve (0-120 μs) with lift-off, measured on corroded and non-corroded regions of a rebar. While the signals show large change with corrosion for low lift-off (<35 mm), the separation is not easily distinguishable at large lift-off. Each box plot comprises of 5 measurements, to capture the variation due to manual method of testing.

The variance explained by each principal component P_i is specified as $VE_{P_i} = \frac{\text{Var}[P_i]}{\sum_{j=1}^M \text{Var}[P_j]}$, where $\text{Var}[P_i]$ is the variance of the i^{th} principal component. The principal components are computed such that the variance shows a decreasing trend, with the highest variance associated with the first principal component. The dominant principal components are found by selecting the components with the highest explained variance VE_{P_i} that cumulatively add up to a pre-determined fraction of the total variance $\sum_{j=1}^M \text{Var}[P_j]$ e.g. 95% [45]. Similarly, the most significant features A_j can be found by selecting features with the highest sum of squared factor loadings i.e. $\sum_{i=1}^M a_{i,j}^2$.

D. Corroded Sample Preparation

The rebars used as test samples in our experiment are artificially corroded by impressed current to induce accelerated corrosion. Naturally occurring corrosion may take months to

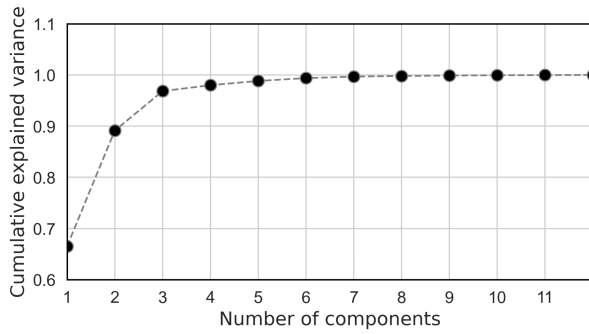


Fig. 5. Cumulative explained variance obtained for PCA with 12 principal components, for features comprising of area under the curve computed for 10 μs long segments of the curve: 0–10 μs , 10–20 μs , ..., 110–120 μs . It is sufficient to represent the data using 3 principal components, that explain 96.8% of the total variance.

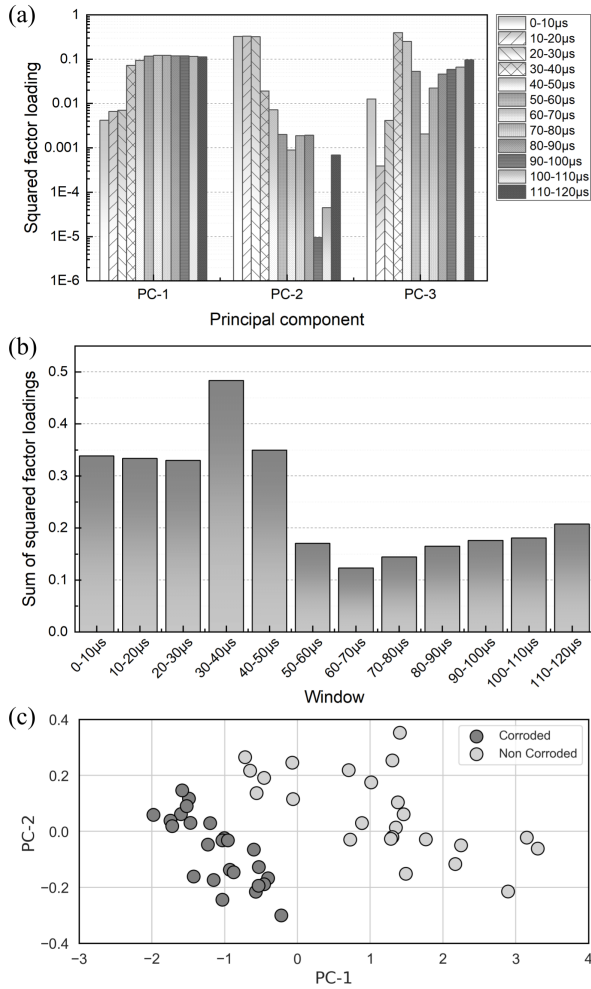


Fig. 6. (a) While we observe an increasing trend in squared factor loadings for component PC-1 and decreasing trend for PC-2, the trend for PC-3 shows a maxima for feature corresponding to time segment 30–40 μs . (b) The sum of squared factor loadings computed for each feature indicate that AUC for 30–40 μs and 40–50 μs are most closely correlated to the principal components. (c) 2D scatter plot showing principal components PC-1 and PC-2 obtained on bare rebar for lift-off ranging from 35 mm to 55 mm, by performing PCA with 2 principal components and 2 features: AUC for 30–40 μs and 40–50 μs .

initiate and even further time for appreciable mass loss to occur. It is also difficult to control the rate of natural corrosion and location of its occurrence. Thus an accelerated corrosion

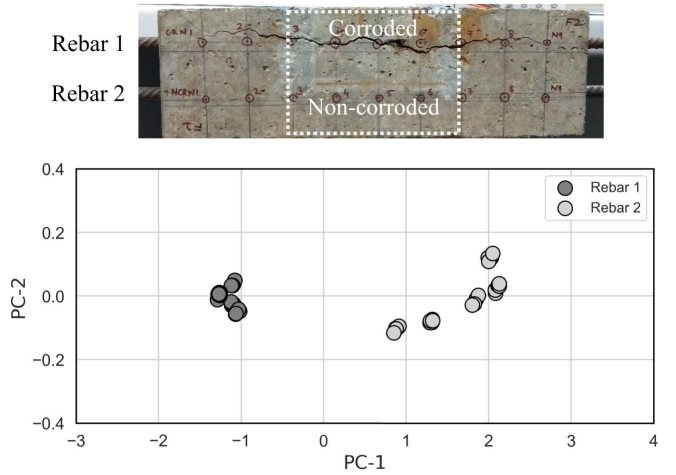


Fig. 7. (Top) Photograph of sample comprising of rebars in concrete subjected to accelerated corrosion. Rebar 1 was corroded using impressed current in the region marked in the figure. (Bottom) PCA visualization for readings obtained on Rebar 1 and Rebar 2 using two principal components obtained for features (AUC) for segments 30–40 μs and 40–50 μs . 25 measurements are taken on each rebar.

setup is used to induce and control localized corrosion of the rebars. The details of the accelerated corrosion setup are described in previous work [46]. The setup comprises of 9% weight by volume NaCl solution used as electrolyte, a copper tube used as cathode, and the rebar to be corroded used as anode. A DC power-supply is used to apply the impressed current to induce corrosion in the rebar. Using the accelerated corrosion setup two samples are prepared: a partially corroded bare rebar, shown in Figure 2(c), and an RCC sample comprising of two rebars embedded in a concrete block with a width of 100 mm depth of 150 mm, and length of 500 mm, one of which is corroded, as shown in Figure 2(d). The thickness of the concrete cover atop these rebars is 50 mm (distance between the axis of the rebar and the concrete surface). For preparing the bare rebar sample, a small section of the 20 mm diameter rebar is corroded such that the average diameter loss in the corroded region is approximately 3 mm. The RCC sample is prepared by corroding one of the rebars embedded in concrete while leaving the other rebar untouched, using the setup detailed in previous work by Sriramadasu *et al.* [46]. Mass loss in the corroded rebar is estimated to be 12%, as determined using Faraday's law of electrolysis. This results in formation of crack on the surface of the concrete. To study the variation in sensor output with extent of corrosion, a steel rebar of 20 mm diameter is manually chamfered at 5 separate locations along its length with a metal grinder. Each chamfered portion is approximately 6 cm long. The average diameter loss of the rebar at these chamfered locations are 7%, 15%, 20%, 31%, and 40%.

III. EXPERIMENTAL RESULTS AND DISCUSSION

Figure 4 shows variation in AUC with lift-off for corroded and non-corroded portions of the bare rebar. The time window used for AUC calculation is 0–120 μs , that captures the entire decaying exponential signal of the sensor. Each box

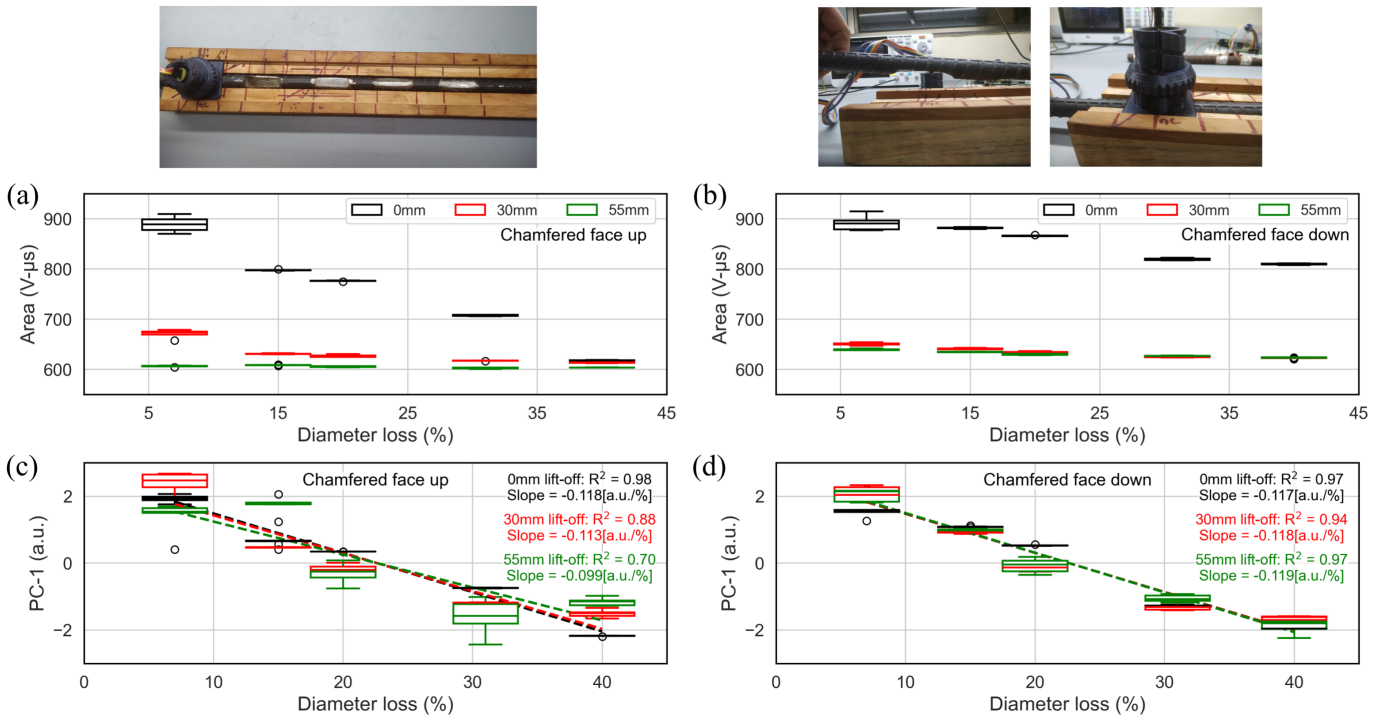


Fig. 8. Variation of AUC (0-120 μs) for chamfered rebar with varying extent of diameter loss, measured for 0 mm, 30 mm and 55 mm lift-off for instances where the chamfered portion is oriented (a) face up, and (b) face down relative to the probe, as shown in accompanying photographs above each figure. (c) & (d) Principal component PC-1 shows linear variation with percentage diameter loss, with similar trend noticed irrespective of sample orientation or lift-off. The principal components are obtained using 2 features: AUC for 30-40 μs and 40-50 μs .

comprises of 5 separate measurements, so as to capture the variation in the sensor output due to manual nature of the test procedure. It is observed that the ability to distinguish between the corroded and non-corroded regions of the rebar diminishes significantly beyond 35 mm lift-off. To extend the sensor capability to distinguish between corroded and non-corroded samples at large lift-off distances, we employ PCA using AUC for various segments of the curves as features for multivariate analysis. The multivariate dataset chosen for the analysis comprises of various segments of the sensor response curve for corroded and non-corroded regions, each of which is 10 μs long: 0-10 μs , 10-20 μs ... 110-120 μs i.e. the dataset is represented using 12 features. PCA is performed using scikit-learn library in python [47], to obtain 12 principal components. The dataset is standardized onto unit scale (i.e. zero mean and unity variance) using the StandardScaler() function in scikit-learn. Figure 5 shows the cumulative explained variance of these principal components. Since the first three principal components explain 96.8% of the variance in the data, we use three principal components (PC-1, PC-2 and PC-3) to identify the most significant features to be used for further analysis.

The correlation of each AUC feature with each principal component is expressed by a loading factor. The square of each loading factor ($a_{i,j}^2$) represents the proportion of variance of the corresponding feature (A_j) explained by the particular principal component (P_i). It is observed that the squared factor loadings show an increasing trend for

component PC-1 and a decreasing trend for PC-2, while the trend for PC-3 shows a maxima for feature corresponding to time segment 30-40 μs (Figure 6(a)). The sum of squared factor loadings for each feature (A_j) across all three principal components (i.e. $\sum_{i=1}^3 a_{i,j}^2$, $j = 1, 2 \dots 12$) signifies the overall variance of the data captured by the feature. This can be used to identify the optimal AUC segments for corrosion analysis. As shown in Figure 6(b), the AUC feature for time segments 30-40 μs and 40-50 μs have the highest sum of squared factor loadings and are therefore chosen for PCA for corrosion analysis. Figure 6(c) shows the output of PCA performed using these two features, represented by two principal components, PC-1 and PC-2, on the dataset comprising of sensor output for corroded and non-corroded regions of the rebar obtained for lift-off values in the range of 35 mm to 55 mm. Unlike the poor resolution offered by AUC of the entire curve as shown in Figure 6(a), PCA results in clearly distinguishable regions in the PC1-PC2 2D space.

Figure 7 shows application of this technique on the rebars embedded in concrete (the concrete cover presents approximately 50 mm lift-off). The middle portion of Rebar-1 shown in the figure is subjected to accelerated corrosion using impressed current as described in previous work [46], resulting in crack formation and discoloration of concrete. Rebar-2 is not corroded, and the distinction between these two rebars is easily visible in Figure 7. While the system is able to adequately distinguish corroded portions of rebars

from non-corroded portions for the samples described above, we also evaluated the sensor performance for the manually chamfered rebar shown in [Figure 2\(e\)](#), to investigate the correlation between the signal features and extent of corrosion. [Figure 8\(a\)](#) shows variation of the AUC for time segment 0-120 μ s for 0 mm, 30 mm and 55 mm lift-off, for measurements obtained with the chamfered portion of the rebar oriented face up relative to the probe as shown (5 measurements in each box in the box-plot). [Figure 8\(b\)](#) shows corresponding measurements obtained with the rebar placed such that the chamfered portion is oriented away (face down) from the probe. While it is possible to visually distinguish the distribution for sensor readings for various percentage diameter loss segments in measurements obtained with 0 mm lift-off, this is not feasible at higher lift-off. However, representing the data at each lift-off using two principal components obtained using AUC feature for time segments 30-40 μ s and 40-50 μ s enhances the resolution of the measurement. When data for each lift-off is standardized onto unit scale, we observe that the first principal component (PC-1) exhibits linear variation with respect to the extent of percentage diameter loss irrespective of orientation of the sample relative to the probe ([Figure 8\(c\)](#) & [\(d\)](#)). This is expected, since standardization using StandardScaler() function involves rescaling the features such that they have the properties of a standard normal distribution [47].

IV. CONCLUSION

In summary, we have presented a novel PEC probe design comprising of an excitation coil and AMR sensor, that enables detection of corrosion in rebars at large lift-off distances (up to 55 mm) with low current (0.2 A). Presently, the probe is capable of introducing maximum lift-off distance of 55 mm, and therefore the analysis presented in this work is limited to 55 mm lift-off. The distinction between corroded and non-corroded samples is magnified by employing PCA to determine optimal segments of the time-domain recording of the sensor output and for representing the data with two most significant principal components. PCA also enables quantitative assessment of extent of diameter loss irrespective of lift-off, as demonstrated with a manually chamfered sample. However, the ability to quantitatively estimate extent of diameter loss using PCA was observed to degrade at higher lift-off, and we aim to explore methods in future work to improve this capability. In future work, we aim to focus on developing the signal analysis further for detection of extent of corrosion of rebars in RCC structures at larger lift-off, methods for automated calibration for rebars of varying diameter, adapting the method to work with a grid of rebars, studying the impact of rebar orientation on sensor output, and prediction of remaining serviceable life based on the sensor output. This will require robust packaging and study of reliability and stability of this solution. We also aim to develop a portable NDT&E embedded system based on this architecture for field testing, in order to study the impact of non-idealities in the field and develop robust algorithms to counter the variation of environmental and operating conditions and their impact on sensor performance.

ACKNOWLEDGMENT

The authors would like to thank Rajeshwara Chary Sriramadasu for discussions on accelerated corrosion of rebars, and staff at Wadhwani Electronics Laboratory (WEL), IIT Bombay, for assistance with component procurement and PCB assembly.

REFERENCES

- [1] E. Allen and J. Iano, *Fundamentals of Building Construction: Materials and Methods*. Hoboken, NJ, USA: Wiley, 2019.
- [2] C. Hansson, "An introduction to corrosion of engineering materials," in *Corrosion of Steel in Concrete Structures*. Amsterdam, The Netherlands: Elsevier, 2016, pp. 3–18.
- [3] G. Koch, J. Varney, N. Thompson, O. Moghissi, M. Gould, and J. Payer, "International measures of prevention, application, and economics of corrosion technologies study," NACE Int., Houston, TX, USA, 2016, Tech. Rep., p. 216.
- [4] *Standard Test Method for Corrosion Potentials of Uncoated Reinforcing Steel in Concrete*, ASTM Int., West Conshohocken, PA, USA, 2003.
- [5] B. Pradhan and B. Bhattacharjee, "Half-cell potential as an indicator of chloride-induced rebar corrosion initiation in RC," *J. Mater. Civil Eng.*, vol. 21, no. 10, pp. 543–552, 2009.
- [6] X. Wang, M. G. Stewart, and M. Nguyen, "Impact of climate change on corrosion and damage to concrete infrastructure in Australia," *Climatic Change*, vol. 110, nos. 3–4, pp. 941–957, Feb. 2012.
- [7] M. G. Stewart, X. Wang, and M. N. Nguyen, "Climate change impact and risks of concrete infrastructure deterioration," *Eng. Struct.*, vol. 33, no. 4, pp. 1326–1337, Apr. 2011.
- [8] D. Luo, Y. Li, J. Li, K.-S. Lim, N. A. M. Nazal, and H. Ahmad, "A recent progress of steel bar corrosion diagnostic techniques in RC structures," *Sensors*, vol. 19, no. 1, p. 34, Dec. 2018.
- [9] A. Fahim, P. Ghods, O. B. Isgor, and M. D. A. Thomas, "A critical examination of corrosion rate measurement techniques applied to reinforcing steel in concrete," *Mater. Corrosion*, vol. 69, no. 12, pp. 1784–1799, Dec. 2018.
- [10] R. Mardaninejad and M. S. Safizadeh, "Gas pipeline corrosion mapping through coating using pulsed eddy current technique," *Russian J. Nondestruct. Test.*, vol. 55, no. 11, pp. 858–867, Nov. 2019.
- [11] J. Valls Miro, N. Ulapane, L. Shi, D. Hunt, and M. Behrens, "Robotic pipeline wall thickness evaluation for dense nondestructive testing inspection," *J. Field Robot.*, vol. 35, no. 8, pp. 1293–1310, Dec. 2018.
- [12] Z. Chu, Z. Jiang, Z. Mao, Y. Shen, J. Gao, and S. Dong, "Low-power eddy current detection with 1-t type magnetoelectric sensor for pipeline cracks monitoring," *Sens. Actuators A, Phys.*, vol. 318, Feb. 2021, Art. no. 112496.
- [13] F. Zhao, D. Chen, Z. Pu, and J. Wang, "A new research method for corrosion defect in metal pipeline by using pulsed eddy current," in *Proc. Pressure Vessels Piping Conf.*, vol. 83877. New York, NY, USA: American Society of Mechanical Engineers, 2020, p. 7, Paper V007T07A012.
- [14] J. García-Martín, J. Gómez-Gil, and E. Vázquez-Sánchez, "Non-destructive techniques based on eddy current testing," *Sensors*, vol. 11, no. 3, pp. 2525–2565, 2011.
- [15] I. Eddy, P. R. Underhill, J. Morelli, and T. W. Krause, "Pulsed eddy current response to general corrosion in concrete rebar," *J. Nondestruct. Eval., Diag. Prognostics Eng. Syst.*, vol. 3, no. 4, Nov. 2020, Art. no. 044501.
- [16] Y. Li, H. Jing, I. Z. Abidin, and B. Yan, "A gradient-field pulsed eddy current probe for evaluation of hidden material degradation in conductive structures based on lift-off invariance," *Sensors*, vol. 17, no. 5, p. 943, Apr. 2017.
- [17] G. Y. Tian and A. Sophian, "Reduction of lift-off effects for pulsed eddy current NDT," *NDT & E Int.*, vol. 38, no. 4, pp. 319–324, 2005.
- [18] F. Nafiah, A. Sophian, M. R. Khan, and I. M. Z. Abidin, "Quantitative evaluation of crack depths and angles for pulsed eddy current non-destructive testing," *NDT & E Int.*, vol. 102, pp. 180–188, Mar. 2019.
- [19] G. Y. Tian and A. Sophian, "Defect classification using a new feature for pulsed eddy current sensors," *NDT & E Int.*, vol. 38, no. 1, pp. 77–82, 2005.
- [20] Z. Xu, X. Wu, J. Li, and Y. Kang, "Assessment of wall thinning in insulated ferromagnetic pipes using the time-to-peak of differential pulsed eddy-current testing signals," *NDT & E Int.*, vol. 51, pp. 24–29, Jul. 2012.

- [21] X. Chen, D. Hou, L. Zhao, P. Huang, and G. Zhang, "Study on defect classification in multi-layer structures based on Fisher linear discriminant analysis by using pulsed eddy current technique," *NDT & E Int.*, vol. 67, pp. 46–54, Oct. 2014.
- [22] N. Ulapane, A. Alempijevic, T. V. Calleja, and J. V. Miro, "Pulsed eddy current sensing for critical pipe condition assessment," *Sensors*, vol. 17, no. 10, p. 2208, 2017.
- [23] I. C. Eddy, P. R. Underhill, J. Morelli, and T. W. Krause, "Pulsed eddy current response to liftoff in different sizes of concrete embedded rebar," in *Proc. IEEE SENSORS*, Oct. 2019, pp. 1–4.
- [24] M. Rourke, Y. Li, and G. Roberts, "Multi-tubular corrosion inspection using a pulsed eddy current logging tool," in *Proc. Int. Petroleum Technol. Conf. (IPTC)*, Houten, The Netherlands: European Association of Geoscientists and Engineers, 2013, p. 350.
- [25] M. Alamin, G. Y. Tian, A. Andrews, and P. Jackson, "Principal component analysis of pulsed eddy current response from corrosion in mild steel," *IEEE Sensors J.*, vol. 12, no. 8, pp. 2548–2553, Aug. 2012.
- [26] F. Nafiah *et al.*, "Parameter analysis of pulsed eddy current sensor using principal component analysis," *IEEE Sensors J.*, vol. 21, no. 5, pp. 6897–6903, Mar. 2021.
- [27] M. Grenier, V. Demers-Carpentier, M. Rochette, and F. Hardy, "Pulsed eddy current: New developments for corrosion under insulation examinations," in *Proc. 19th World Conf. Non-Destructive Testing*, Munich, Germany, 2016, pp. 13–17.
- [28] M. Morozov, G. Dobie, and A. Gachagan, "Assessment of corrosion under insulation and engineered temporary wraps using pulsed eddy-current techniques," in *Proc. 56th Annu. Conf. Brit. Inst. Non-Destructive Test.*, 2017, pp. 475–484.
- [29] C. P. Dolabdjian, L. Perez, V. O. De Haan, and P. A. De Jong, "Performance of magnetic pulsed-eddy-current system using high dynamic and high linearity improved giant magnetoresistance magnetometer," *IEEE Sensors J.*, vol. 6, no. 6, pp. 1511–1517, Dec. 2006.
- [30] N. Ulapane, S. Wickramanayake, and S. Kodagoda, "Pulsed eddy current sensing for condition assessment of reinforced concrete," in *Proc. 14th IEEE Conf. Ind. Electron. Appl. (ICIEA)*, Jun. 2019, pp. 1–6.
- [31] V. G. M. Annadass, S. Bhalla, and C. K. Soh, "Applications of structural health monitoring technology in Asia," *Struct. Health Monit.*, vol. 16, no. 3, pp. 324–346, May 2017.
- [32] S. Xie, Z. Chen, T. Takagi, and T. Uchimoto, "Quantitative non-destructive evaluation of wall thinning defect in double-layer pipe of nuclear power plants using pulsed ECT method," *NDT & E Int.*, vol. 75, pp. 87–95, Oct. 2015.
- [33] G. Piao, J. Guo, T. Hu, Y. Deng, and H. Leung, "A novel pulsed eddy current method for high-speed pipeline inline inspection," *Sens. Actuators A, Phys.*, vol. 295, pp. 244–258, Aug. 2019.
- [34] I. Z. Abidin, C. Mandache, G. Y. Tian, and M. Morozov, "Pulsed eddy current testing with variable duty cycle on rivet joints," *NDT & E Int.*, vol. 42, no. 7, pp. 599–605, 2009.
- [35] X. Chen and X. Liu, "Pulsed eddy current-based method for electromagnetic parameters of ferromagnetic materials," *IEEE Sensors J.*, vol. 21, no. 5, pp. 6376–6383, Mar. 2021.
- [36] D. P. Johnston, J. A. Buck, P. R. Underhill, J. E. Morelli, and T. W. Krause, "Pulsed eddy-current detection of loose parts in steam generators," *IEEE Sensors J.*, vol. 18, no. 6, pp. 2506–2512, Mar. 2018.
- [37] L. Xie, B. Gao, G. Y. Tian, J. Tan, B. Feng, and Y. Yin, "Coupling pulse eddy current sensor for deeper defects NDT," *Sens. Actuators A, Phys.*, vol. 293, pp. 189–199, Jul. 2019.
- [38] C. S. Angani, D. G. Park, G. D. Kim, C. G. Kim, and Y. M. Cheong, "Differential pulsed eddy current sensor for the detection of wall thinning in an insulated stainless steel pipe," *J. Appl. Phys.*, vol. 107, no. 9, 2010, Art. no. 09E720.
- [39] B. Lebrun, Y. Jayet, and J.-C. Baboux, "Pulsed eddy current signal analysis: Application to the experimental detection and characterization of deep flaws in highly conductive materials," *NDT & E Int.*, vol. 30, no. 3, pp. 163–170, 1997.
- [40] P. Li *et al.*, "A novel frequency-band-selecting pulsed eddy current testing method for the detection of a certain depth range of defects," *NDT & E Int.*, vol. 107, Oct. 2019, Art. no. 102154.
- [41] K. Tsukada *et al.*, "Detection of inner corrosion of steel construction using magnetic resistance sensor and magnetic spectroscopy analysis," *IEEE Trans. Magn.*, vol. 52, no. 7, pp. 1–4, Jul. 2016.
- [42] D. F. He, M. Tachiki, and H. Itozaki, "Highly sensitive anisotropic magnetoresistance magnetometer for eddy-current nondestructive evaluation," *Rev. Sci. Instrum.*, vol. 80, no. 3, Mar. 2009, Art. no. 036102.
- [43] W. Cheng, "Pulsed eddy current testing of carbon steel pipes' wall-thinning through insulation and cladding," *J. Nondestruct. Eval.*, vol. 31, no. 3, pp. 215–224, Sep. 2012.
- [44] C. P. Bean, R. W. DeBlois, and L. B. Nesbitt, "Eddy-current method for measuring the resistivity of metals," *J. Appl. Phys.*, vol. 30, no. 12, pp. 1976–1980, Dec. 1959.
- [45] I. T. Jolliffe, *Principal Component Analysis* (Springer Series in Statistics), vol. 29. New York, NY, USA: Springer-Verlag, 2002.
- [46] R. C. Sriramadasu, Y. Lu, and S. Banerjee, "Identification of incipient pitting corrosion in reinforced concrete structures using guided waves and piezoelectric wafer transducers," *Struct. Health Monit.*, vol. 18, no. 1, pp. 164–171, Jan. 2019.
- [47] F. Pedregosa *et al.*, "Scikit-learn: Machine learning in Python," *J. Mach. Learn. Res.*, vol. 12, pp. 2825–2830, Oct. 2011.



Durgesh Tamhane received the M.Sc. degree in physics from the University of Mumbai, Mumbai, India, in 2011. He is currently pursuing the Ph.D. degree in electrical engineering at IIT Bombay, and his thesis research focuses on design and development of sensors for SHM. From 2015 to 2017, he worked as a Project Research Assistant at NMPF, Department of Electrical Engineering, IIT Bombay. He has won the IEEE International Sensors and Measurement Student Contest at 2018 and 2019 IEEE Sensors conferences.



Jinit Patil received the B.E. degree in instrumentation engineering from Vidyavardhini's College of Engineering and Technology, Mumbai University, Mumbai, India, in 2017, and the M.Tech. degree in electrical engineering at IIT Bombay, specializing in electronic systems. His research interests include embedded systems and robotics.



Sauvik Banerjee is a Professor of Structural Engineering with the Department of Civil Engineering, IIT Bombay. Prior to joining IIT Bombay, he was an Assistant Professor with the Parks College of Engineering, Aviation and Technology, Saint Louis University, USA. He has more than 100 publications, several awards, and has been a PI for several sponsored research and industrial consultancy projects worth over USD 2 million. His research interests include SHM using wave propagation and vibration-based approaches, ultrasonic NDE of materials, and elastodynamic modeling of advanced composite structures. He is currently an Associate Editor of *Journal of Nondestructive Evaluation, Diagnostics and Prognostics of Engineering Systems* (ASME).



Siddharth Tallur received the B.Tech. degree in electrical engineering at IIT Bombay in 2008, and the M.S. and Ph.D. degrees in electrical and computer engineering from Cornell University in 2011 and 2013, respectively. He is an Associate Professor with the Department of Electrical Engineering, IIT Bombay. Previously, he worked at Analog Devices Inc., Wilmington, MA, USA, as an MEMS Products and Applications Engineer from 2013 to 2016. His research interests include high resolution and low cost physical and biosensors and high speed instrumentation and embedded systems for sensing applications.